



Article

# The Influence of Nitrogen Flow Rate on the Structure and Properties of Mo-Hf-Y-Si-B-N Coatings

Philipp Kiryukhantsev-Korneev <sup>1,\*</sup> , Alina Sytchenko <sup>1,\*</sup> , Fedor Chudarin <sup>1</sup>, Boris Senatulin <sup>2</sup> and Evgeny Levashov <sup>1</sup>

<sup>1</sup> Laboratory “In Situ Diagnosis of Structural Transformations” of the Scientific—Educational Center of SHS, National University of Science and Technology MISIS, 119049 Moscow, Russia

<sup>2</sup> Joint Research Center «Material Science and Metallurgy», National University of Science and Technology MISIS, 119049 Moscow, Russia; borisrs@yandex.ru

\* Correspondence: kiruhancev-korneev@yandex.ru (P.K.-K.); alina-sytchenko@yandex.ru (A.S.); Tel.: +7-(495)-638-46-59 (P.K.-K. & A.S.)

**Abstract:** This work is devoted to the production of Mo-Hf-Y-Si-B-N coatings using magnetron sputtering with varying N<sub>2</sub> flow rate; the analysis of magnetron discharge plasma; and the investigation of the structure, and optical, mechanical, and tribological characteristics, as well as crack resistance and oxidation resistance, of the coatings. The results show that Mo-Hf-Y-Si-B-N coatings were characterized by a dense, homogeneous structure. The non-reactive coatings had a maximum growth rate of 270 nm/min. An increase in the flow rate of N<sub>2</sub> from 0 to 37.5 sccm led to a decrease in the growth rate by 5.4 times. Mo-Hf-Y-Si-B-N coatings were X-ray amorphous. In non-reactive coatings, the presence of Mo-Si and Mo-B bonds was revealed. The introduction of nitrogen contributed to the formation of an additional Si-N bond, an increase in the proportion of which led to an increase in transmittance. The Mo-Hf-Y-Si-B coating was characterized by a hardness value of 14 GPa. The maximum hardness of 16 GPa was observed in coatings obtained at nitrogen flow rates of 12.5 and 25.0 sccm. A further increase in the consumption of N<sub>2</sub> to 37.5 sccm led to a decrease in hardness by 38%. The coating obtained at a flow rate of 25 sccm N<sub>2</sub> was characterized by maximum elastic recovery of 57%, elastic strain to failure of 0.098, and resistance to plastic deformation of 0.157 GPa. An increase in nitrogen flow rate from 0 to 12.5 sccm contributed to a decrease in the wear rate of coatings under sliding friction conditions by 40%. The non-reactive Mo-Hf-Y-Si-B coating had the best oxidation resistance at 1000 °C.

**Keywords:** MoSi<sub>2</sub>-based coatings; magnetron sputtering; structure and phase composition; mechanical properties; oxidation resistance



**Citation:** Kiryukhantsev-Korneev, P.; Sytchenko, A.; Chudarin, F.; Senatulin, B.; Levashov, E. The Influence of Nitrogen Flow Rate on the Structure and Properties of Mo-Hf-Y-Si-B-N Coatings. *J. Compos. Sci.* **2023**, *7*, 253. <https://doi.org/10.3390/jcs7060253>

Academic Editor: Prashanth Konda Gokuldoss

Received: 21 March 2023

Revised: 8 June 2023

Accepted: 15 June 2023

Published: 17 June 2023



**Copyright:** © 2023 by the authors. Licensee MDPI, Basel, Switzerland. This article is an open access article distributed under the terms and conditions of the Creative Commons Attribution (CC BY) license (<https://creativecommons.org/licenses/by/4.0/>).

## 1. Introduction

The development of new samples with modern techniques under conditions where the potential of consolidated materials has been reached is impossible without the use of surface modification technologies and the creation of functional coatings. At present, considerable attention is being paid to research on oxidation-resistant coatings for the protection of critical products exposed to high temperatures and aggressive gas environments, as well as various types of wear.

Some of the most promising coatings are those based on refractory metal silicides. Among the ion-plasma coatings, such as TaSi<sub>2</sub>, NbSi<sub>2</sub>, and MoSi<sub>2</sub>, MoSi<sub>2</sub> has the best characteristics and successfully retains its protective properties at 1200 °C for 100 h exposure [1]. In the laboratory of J.H. Perepetsko, a two-stage technology, including the deposition of molybdenum from the gas phase followed by the pack cementation of Si and B, is used to obtain MoSiB coatings, which have high oxidation resistance at temperatures up to 1300 °C [2,3]. The main achievements in the field of creating heat-resistant and oxidation-resistant bulk ceramic materials and coatings in the MoSiB system are considered

in the review [4]. Among domestic developments, it is worth mentioning the studies on multicomponent coatings based on molybdenum disilicide with a complex multilevel architecture conducted under the guidance of prof. V.S. Terent'eva [5]. The developed coatings briefly resist oxidation in ionized air flows up to 1800–2100 °C.

For MeSiN (Me: Mo, Zr, or Ta) nitride coatings with a high silicon concentration, satisfactory oxidation resistance was achieved at temperatures up to 1300 °C [6]. Important results from the point of view of practical applications were obtained by the group of prof. J. Vlcek in the development of coatings in the SiBCN system [7,8]. SiBCN thin-film coatings have not only high oxidation resistance but also high thermal stability up to a temperature of 1700 °C inclusive. The next round of research included the creation of SiBCN coatings doped with hafnium and rare earth metals: HfBSiCN with oxidation resistance up to 1600 °C [9], and HfYSiBCN [10] and HfHoSiBCN [11] with thermal stability and oxidation resistance up to 1300 °C and higher. In parallel, investigations were carried out on ZrSiB/SiBC [12] and MoSiB/SiBC [13] multilayer coatings providing oxidation resistance up to 1200 °C and 1500 °C, respectively. Comparative studies on TM-Si-B coatings (TM (transition metal): Ti, Cr, Hf, Ta, or W) confirmed the promise of compositions based on hafnium [14].

In our laboratory, using the direct current magnetron sputtering method and multi-phase cathodes, the following coatings were obtained: ZrSiB with oxidation resistance up to 1500 °C [12]; MoSiB, up to 1700 °C [15]; and MoHfZrSiB, up to 1500 °C [16]. In addition, a hybrid technology that combines the electrospark alloying of a heat-resistant nickel alloy with the subsequent deposition of a MoSiB layer using magnetron sputtering has been successfully applied [17].

For practical applications, it is important to provide coatings with not only high oxidation resistance but also high wear resistance. It is known that alloying with nitrogen by modifying the structure of ion-plasma coatings, including boride and silicide coatings, promotes an increase in adhesive strength, crack resistance, and tribological properties under various friction conditions [18,19]. For example, in HfMoSiN coatings, the addition of nitrogen due to the formation of an amorphous Si<sub>3</sub>N<sub>4</sub> phase increases crack resistance and fracture toughness, which ensures high values of the parameters H/E (0.14), H<sup>3</sup>/E<sup>2</sup> (0.61 GPa), low friction coefficient (0.37), and wear rate (1.8 × 10<sup>-6</sup> mm<sup>3</sup>N<sup>-1</sup>m<sup>-1</sup>) [20]. Taking into account the high oxidation resistance of MoHfZrSiB coatings and the positive effect of nitrogen on the tribological characteristics, it is promising to develop coatings in the Mo-Hf-Y-Si-B-N system. It should be noted that no works on obtaining and studying coatings in the Mo-Hf-Y-Si-B-N system have been previously carried out.

Coatings based on Mo-Si-B are usually obtained by means of carburizing [3,21], spark plasma sintering [22], plasma spraying [23], electrospark deposition [24], and magnetron sputtering [13,15–17]. Among all technologies, magnetron sputtering is recognized as one of the most promising, since it preserves the substrate geometry and makes it possible to obtain coatings with low roughness, residual porosity, and defect concentration; high adhesion; and a uniform distribution of elements along the coating depth [16,18,25].

The aim of this work was to study the effect of nitrogen addition on the structural, mechanical, and tribological properties, as well as resistance to high-temperature oxidation, of Mo-Hf-Y-Si-B-N coatings deposited using magnetron sputtering.

## 2. Materials and Methods

Coatings were deposited using a modernized UVN-2M installation, in the working space of which a magnetron and a source of gas ions were located [16]. An 80% (90% MoSi<sub>2</sub> + 10% MoB) + 20% HfB<sub>2</sub> composite disk target with a diameter of 120 mm in the erosion zone of which there were yttrium (99.5%) segments for a total area of 10.0 cm<sup>2</sup> was subjected to direct current magnetron sputtering. The substrate-magnetron distance was 8 cm. The power in all experiments was maintained at the level of 1 kW (500 V, 2 A) using a Pinnacle+ 5 × 5 power supply (Advanced Energy, Denver, CO, USA). The coatings were deposited in an Ar medium (99.9995%) and in gas mixtures of Ar and N<sub>2</sub> (99.999%).

The operating gas pressure of 0.2 Pa was maintained. The residual pressure in the chamber was  $3 \times 10^{-3}$  Pa. The gas flow was controlled with a three-channel gas supply system. When applying nitrogen-containing coatings, the flow rate of  $N_2$  was 0, 12.5, 25.0, or 37.5 sccm. No bias voltage was supplied to the substrate during coating deposition. Coatings were deposited on single-crystal silicon, polycrystalline alumina, glass, and stainless-steel substrates. Substrate preparation included ultrasonic cleaning in isopropanol using an UZDN-2T unit and etching with  $Ar^+$  ions (2.5 kV, 80 mA,  $8 \times 10^{-2}$  Pa, 10 min) in a vacuum chamber before coating deposition. The coating deposition time was 10 min. The magnetron discharge plasma was studied with optical emission spectroscopy using a PlasmaScope spectrometer (Horiba Jobin Yvon, Longjumeau, France). The optical signal was fed to the spectrometer via a quartz fiber with a collimator located at a distance of 10 cm from the disk magnetron parallel to its plane.

The composition and structure of the coatings were studied with scanning electron microscopy (SEM) using an S-3400 (Hitachi, Tokyo, Japan) instrument equipped with a Noran-7 energy-dispersive spectrometer (EDS) (Thermo Fisher Scientific, Waltham, MA, USA). The distribution profiles of elements over the thickness of the coatings were obtained using glow discharge optical emission spectroscopy (GDOES) with a Profiler-2 spectrometer (Horiba Jobin Yvon, Longjumeau, France) [26]. Phase composition was estimated using X-ray diffraction (XRD) (D2 Phaser; Bruker, Karlsruhe, Germany) and Raman spectroscopy (NTEGRA; NT-MDT, Zelenograd, Russia). X-ray photoelectron spectroscopy (XPS) studies were conducted with a PHI5000 VersaProbe II instrument using monochromatic  $Al K\alpha$  radiation ( $h\nu = 1486.6$  eV) as an excitation source (power, 50 W; diameter, 200  $\mu m$ ). The area of the analyzed region was  $800 \times 200 \mu m^2$ . The high-resolution spectra were recorded at the pass energy of 23.5 eV and the step size of 0.2 eV. The spectra were fitted with the nonlinear least-squares technique using the Gaussian and Lorentzian functions. Scanning was performed after ion etching ( $Ar^+$  ions with energy of 1 keV) for 6 min. Roughness was determined using the optical profilometer WYKO NT1100 (Veeco, Plainview, NY, USA).

The nanoindentation method (Nanonardness Tester; CSM Instruments, Peseux, Switzerland) was used to determine hardness (H), elastic modulus (E), and elastic recovery (W) at the load of 4 mN. Residual stress in the coating was evaluated by measuring the curvature of the substrate before and after the deposition of the coating using the Stoney formula [27]. Curvature measurements were performed using a WYKO-NT1100 optical profilometer. The crack resistance and adhesive strength of the coatings were determined after indentation at loads of 0.5–2 N (Durascan; EMCO-TEST PrufmaSchinen GmbH, Kuchl, Austria) and 10–50 N (HVS-50; Time Group Inc., Beijing, China). The sliding friction tests of the coatings were carried out according to the “pin-on-disk” scheme using an HT tribometer (CSM Instruments). An  $Al_2O_3$  ball of 6 mm in diameter was used as a counterbody. The load was 1 N. The tribocontact zones were studied using a WYKO NT1100 optical profilometer; the wear rate (Vw) was then calculated using the following formula:

$$V_w = V / (F \times L) \quad (1)$$

where V is the volume of the wear track,  $mm^3$ ; F is the normal load, N; and L is the friction distance, m. The friction distance was calculated using  $L = 2\pi r$ , where r is the wear track radius.

The kinetics of coating oxidation were evaluated by annealing in an SNOL 7.2/1200 furnace (AB “UMEGA”; Utena, Lithuania) at a temperature of 1000 °C and holding times of 10–180 min.

### 3. Results and Discussions

On the plasma spectra (Figure 1) recorded during the deposition of coatings, the main peaks observed were those of the ions of the target components:  $Mo^{n+}$ ,  $Si^{n+}$ ,  $B^+$ ,  $Hf^{n+}$ , and  $Y^{n+}$  at positions 390.1, 288.2, 249.1, 286.6, and 377.5 nm, respectively.

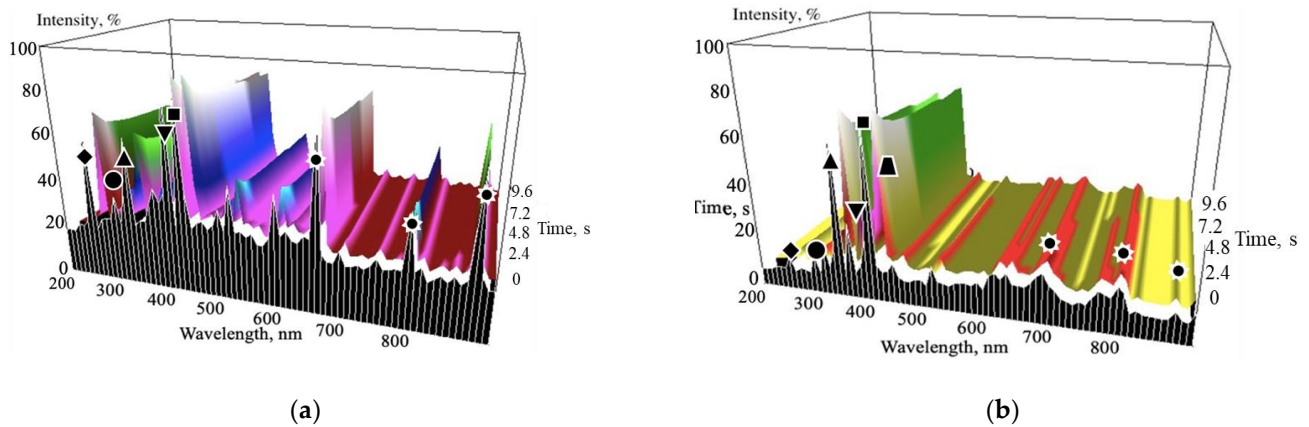


**Figure 1.** Plasma spectra recorded during (MoSi<sub>2</sub> + 10% MoB) + 20% HfB<sub>2</sub> + 4Y target sputtering at nitrogen flow rates of 0 (a) and 37.5 sccm (b).

During non-reactive deposition, the spectra at wavelengths of 690, 810, and 900 nm exhibited high-intensity peaks corresponding to Ar<sup>+</sup>. The introduction of nitrogen into the composition of the gaseous medium led to the appearance of new peaks at 336.8, 357.0, 391.1, and 423.2 nm, corresponding to N<sup>n+</sup> ions. An increase in nitrogen flow rate from 12.5 to 37.5 sccm contributed to an increase in the intensity of N<sup>n+</sup> peaks by three times. Naturally, we had expected an increase in nitrogen content in the same proportions. When passing from non-reactive (Ar) to reactive deposition (37.5 sccm N<sub>2</sub>), a decrease in the intensity of the Mo<sup>n+</sup>, Si<sup>n+</sup>, B<sup>+</sup>, Hf<sup>n+</sup>, and Y<sup>n+</sup> peaks by 1.2–1.3 times was observed. A decrease in the concentration of argon ions in the plasma with an increase in the flow rate of nitrogen from 0 to 37.5 sccm affected the growth rate of the coatings.

According to the GDOES profiles, all elements in the coatings were distributed uniformly along the depth (Figure 2a,b).

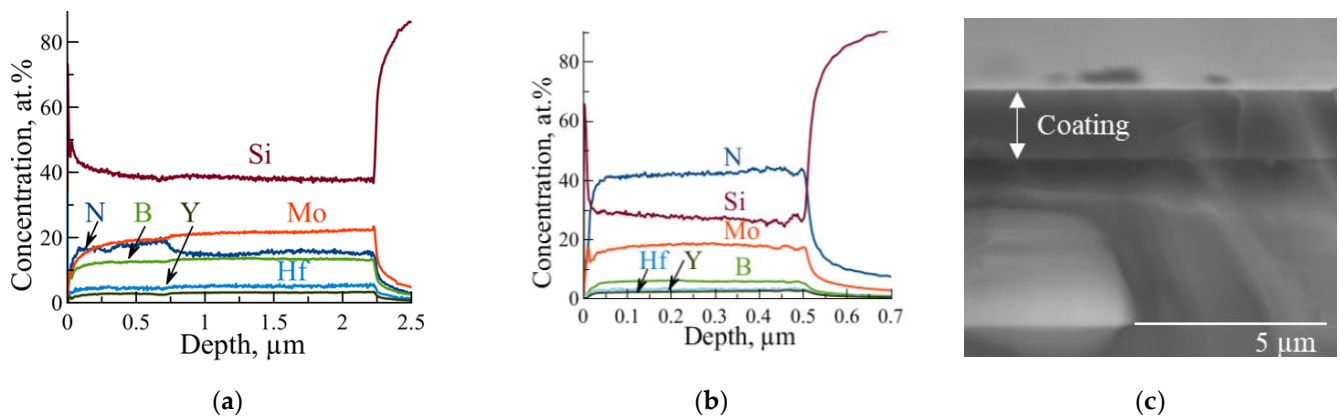


**Figure 2.** Elemental profiles of coatings obtained at 12.5 (a) and 37.5 sccm N<sub>2</sub> (b). Cross-section SEM image of the coating deposited at 12.5 sccm N<sub>2</sub> (c).

The thickness values were determined from the GDOES elemental profiles, and the growth rates of the coatings were calculated (Table 1).

The non-reactive Mo-Hf-Y-Si-B coating was characterized by maximal thickness of 2.7 μm and growth rate of 270 nm/min. Increasing the nitrogen flow rate to 12.5, 25.0, and 37.5 sccm led to a decrease in thickness and growth rate by 1.1, 1.4, and 5.4 times, respectively. A decrease in the growth rate can be associated with the poisoning of the target by the reaction gas and the formation of a nitrogen-containing layer on its surface [28], as well as with a lower nitrogen ionization coefficient compared with Ar and the scattering of sputtered atoms by heavier molecules of nitrogen [29].

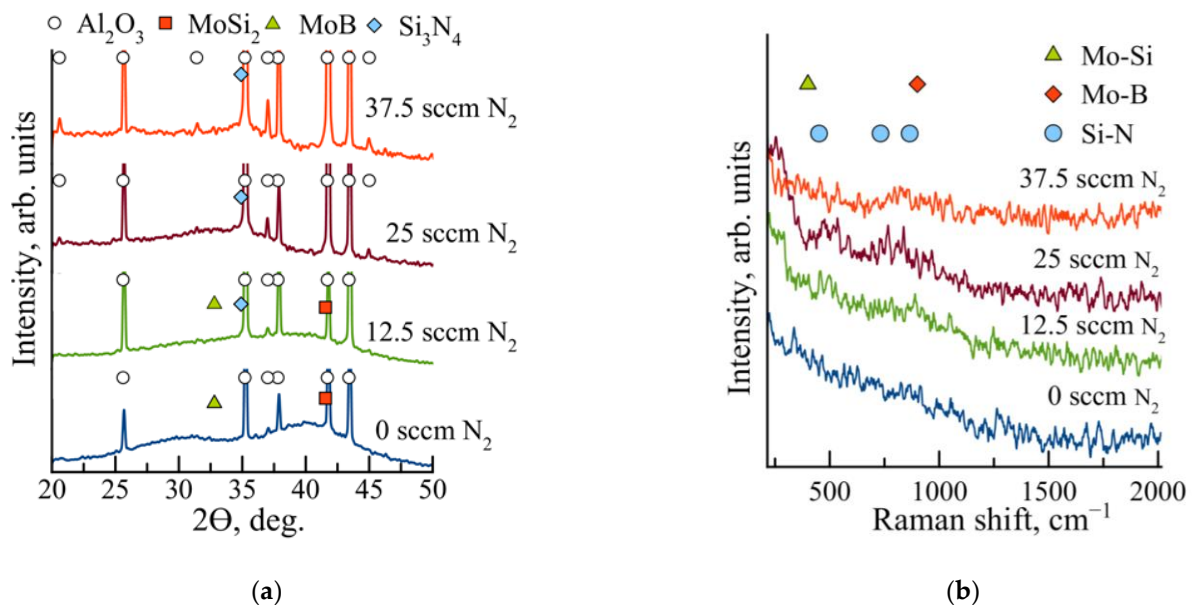
**Table 1.** Deposition regime, thickness, growth rate, and elemental composition of coatings.

Gas Flow Rate, sccm		Elemental Composition, at.%						Thickness, $\mu\text{m}$	Growth Rate, nm/min
Ar	N <sub>2</sub>	Mo	Si	B	Y	Hf	N		
37.5	0	27.1 $\pm$ 1.0	45.8 $\pm$ 1.1	17.2 $\pm$ 0.2	4.1 $\pm$ 0.1	6.8 $\pm$ 0.3	0	2.7	270
25.0	12.5	22.7 $\pm$ 1.2	39.8 $\pm$ 0.5	13.7 $\pm$ 0.5	3.1 $\pm$ 0.2	5.3 $\pm$ 0.3	15.4 $\pm$ 1.2	2.5	250
12.5	25.0	17.7 $\pm$ 0.7	37.5 $\pm$ 0.6	7.4 $\pm$ 0.1	2.5 $\pm$ 0.1	3.5 $\pm$ 0.2	31.4 $\pm$ 0.9	2.0	200
0	37.5	17.4 $\pm$ 0.5	27.9 $\pm$ 0.9	5.8 $\pm$ 0.1	2.5 $\pm$ 0.1	3.2 $\pm$ 0.2	43.2 $\pm$ 0.8	0.5	50

The elemental composition of the coatings, averaged over the thickness, is presented in Table 1. As the N<sub>2</sub> flow rate increased from 0 to 12.5, 25.0, and 37.5 sccm, the nitrogen concentration in the coatings increased from 0 to 15.4, 31.4, and 43.2 at.%, respectively. At the same time, the concentration of the main elements, Mo, Si, Hf, and B, decreased. The content of Y in the coatings was in the range of 2–4 at.%. It should be noted that the Mo:Si ratios of the coatings obtained at 0 and 12.5 sccm N<sub>2</sub> were close and amounted to 0.58. An excess of Mo can form MoB phase by analogy with our previous experiments in research on coatings in the Mo-Si-B system [13,15,16]. An increase in the nitrogen concentration in the coatings can promote the formation of BN, MoN, and/or Si<sub>3</sub>N<sub>4</sub> phases. According to the difference in the Gibbs energies of BN ( $\Delta G_0 = -226.8$  kJ/mol), MoN ( $\Delta G_0 = -100.4$  kJ/mol), and Si<sub>3</sub>N<sub>4</sub> ( $\Delta G_0 = -647.7$  kJ/mol) phases determined using FactWeb software, nitrogen-containing Si<sub>3</sub>N<sub>4</sub> phase should predominantly form.

Figure 2c shows a typical cross-section SEM image of the coatings obtained at 12.5 sccm N<sub>2</sub>. It can be seen that the coatings had a homogeneous defect-free microstructure without pronounced columnar elements, which is usually observed for two- and three-component coatings, such as Mo-N and Mo-Si-N [30]. The coatings demonstrated the same level of roughness, and the Ra parameter was in range of 9–12 nm. The Al<sub>2</sub>O<sub>3</sub> substrate roughness was ~10 nm.

According to XRD data, all coatings were X-ray amorphous (Figure 3a).

**Figure 3.** XRD patterns (a) and Raman spectra (b) of Mo-Hf-Y-Si-B-N coatings.

For the Mo-Hf-Y-Si-B coating, two broad peaks were observed at positions  $2\theta = 25\text{--}33$  and  $35\text{--}45^\circ$ , the maxima of which were close to the position of the most intense lines, (103) and (111), of t-MoB phase (ICDD 73-1768) and h-MoSi<sub>2</sub> phase (ICDD 80-4771), respectively. The introduction of nitrogen into the coating composition led to a shift in the amorphous

halo towards smaller angles, which may be associated with the formation of amorphous  $a\text{-Si}_3\text{N}_4$  phase. It can be noted that the  $t\text{-Si}_3\text{N}_4$  crystalline phase (ICDD 40-1129) has the main peak at  $2\Theta = 34.9^\circ$ , corresponding to the (320) line with an interplanar spacing of 0.257 nm.

Raman spectra made it possible to refine the phase composition of the X-ray amorphous Mo-Hf-Y-Si-B-N coatings (Figure 3b). For the non-reactive coating, peaks were detected at positions  $400$  and  $970\text{ cm}^{-1}$ , corresponding to Mo-Si [31] and Mo-B [32] bonds. An increase in nitrogen consumption led to the formation of the Si-N bond in the Mo-Hf-Y-Si-B-N coatings, the peaks of which were observed at positions  $450$ ,  $730$ , and  $860\text{ cm}^{-1}$  [33].

For a better understanding of the chemical arrangement, the XPS method was used. Figure 4 shows the high-resolution N1s, Si2p, Mo3d, and B1s spectra taken from Mo-Y-Si-B-N coatings obtained at  $37.5\text{ sccm N}_2$ . The spectrum of N1s showed an intense peak at  $397.3\text{ eV}$  corresponding to B-N ( $396.7\text{ eV}$ ) [34] and Si-N ( $397.5\text{ eV}$ ) [35]. The Mo3d spectrum contained two main doublets described by the  $3d_{5/2}$  and  $3d_{3/2}$  states. Peaks corresponding to binding energies of  $227.6$  and  $230.8\text{ eV}$  indicate that molybdenum is chemically bonded to silicon [36,37]. Low-intensity peaks at positions  $228.8$  and  $232.3\text{ eV}$  correspond to Mo-O bonds [38]. According to the B1s spectra, B-N bonds were also present in the coatings [34]. The Si2p spectrum with maxima at positions  $101.8\text{ eV}$  and  $102.9\text{ eV}$  confirmed the presence of Si-N and Si-O bonds [39,40]. A peak at the binding energy of  $99.6\text{ eV}$  corresponds to molybdenum silicide [41]. Thus, Mo-Si and Mo-B bonds were present in the coatings, and yttrium atoms were predominantly bonded to silicon and oxygen atoms.

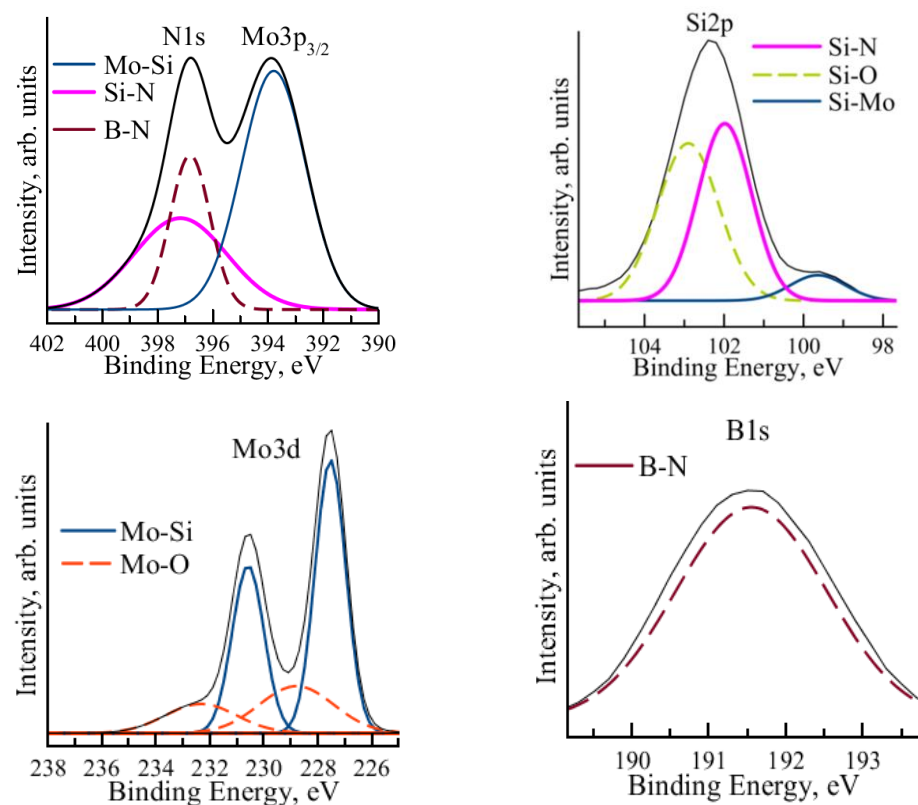


**Figure 4.** High-resolution N1s, Si2p, Mo3d, and B1s spectra taken from coatings obtained at  $37.5\text{ sccm N}_2$ .

The spectrophotometric studies showed that with an increase in nitrogen consumption, an increase in transmittance (T) occurred (Supplementary Materials Figure S1), which can be explained both by a decrease in the thickness of the coatings and an increase in the proportion of non-metallic bonds.

In the case of Mo-Hf-Y-Si-B-N coatings containing the maximum concentration of nitrogen (45 at.%), an increase in optical transmittance from 2 to 12% was observed with the increase in wavelength from 450 to 950 nm.

The results of the nanoindentation of Mo-Hf-Y-Si-B-N coatings are shown in Figure 5.

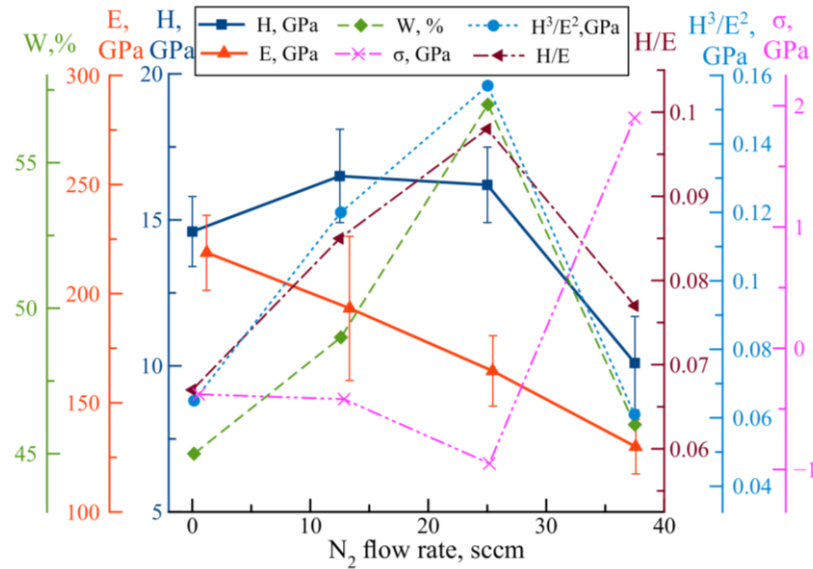


**Figure 5.** Dependence of mechanical properties of Mo-Hf-Y-Si-B-N coatings on N<sub>2</sub> flow rate.

The Mo-Hf-Y-Si-B coating was characterized by hardness  $H = 14$  GPa. The maximal value of  $H = 16$  GPa was seen in coatings obtained at nitrogen flow rates of 12.5 and 25.0 sccm. An increase in the N<sub>2</sub> flow rate from 25.0 to 37.5 sccm led to a decrease in hardness to 10 GPa, which was associated with an increase in the volume fraction of the amorphous component. A similar dependence was observed in Mo-Al-Si-N coatings; the highest hardness was achieved at a N<sub>2</sub> flow rate of 15 sccm, which the authors associated with the formation of a nanocomposite structure and the optimal crystallite size [42]. For Mo-Hf-Y-Si-B-N coatings, a linear dependence of the elastic modulus ( $E$ ) on nitrogen consumption was established:  $E$  decreased from 220 to 130 GPa with the increase in nitrogen consumption from 0 to 37.5 sccm. The decrease in  $E$  can be associated with the increase in the content of the amorphous component ( $a\text{-Si}_3\text{N}_4$ ) in nitrogen-containing coatings [43] ( $E = 313$  GPa for  $\text{Si}_3\text{N}_4$  [44] versus  $E = 388$  GPa for  $\text{MoSi}_2$  [45]). Extremal dependence of elastic recovery ( $W$ ), elastic strain to failure ( $H/E$ ), and resistance to plastic deformation ( $H^3/E^2$ ) on nitrogen consumption was observed (Figure 4). The maximal values of  $W = 57\%$ ,  $H/E = 0.098$ , and  $H^3/E^2 = 0.157$  GPa were achieved at a N<sub>2</sub> flow rate of 25 sccm, which may have been due to the high level of internal compressive stress ( $\sigma$ ) of  $-0.95$  GPa (Figure 4). It should be noted that a high level of internal stress is characteristic of reactive nitrogen-containing coatings [18].

For the practical application of coatings, it is important to study the crack resistance of coatings and wear resistance under conditions of sliding friction.

A study of the crack resistance of Mo-Hf-Y-Si-B-N coatings deposited onto a steel substrate when indented with a Vickers pyramid under loads of 10 and 50 N showed that no cracks were observed along the indentation boundaries in all coatings in the entire range of loads (Supplementary Materials Figure S2). It should be noted that Mo-Si-N coatings obtained on a steel substrate crack even at a load of 1 N [46]. In the case of the non-reactive Mo-Hf-Y-Si-B coating, no delaminations along the indentation boundaries were observed in the entire load range. In the coating obtained at a N<sub>2</sub> flow rate of 12.5 sccm, at a load of 10 N, no damage was found in the indentation zone. When the load was increased to 50 N, areas of delamination of the coating were observed in the corners of the imprint. The coating deposited at 25 sccm N<sub>2</sub> peeled off along the indentation boundaries at loads of 10 and 50 N, which may have been due to high levels of internal stress. It was shown in [47]

that a high level of residual stress in coatings reduces their adhesive strength and affects the nature of failure. The coating deposited at the maximal nitrogen flow rate was not destroyed during indentation at loads of 10 and 50 N.

Tribological tests in sliding friction mode showed that the coatings obtained on Al<sub>2</sub>O<sub>3</sub> substrates at nitrogen flow rates of 0 and 12.5 sccm showed close values of friction coefficient  $f = 0.90 \pm 0.03$  (Figure 6). Increases in nitrogen flow rate to 25 and 37.5 sccm led to increases in the friction coefficient to  $0.98 \pm 0.02$  and  $1.02 \pm 0.03$ , respectively. A study of the wear tracks using optical profilometry showed that the wear rate (Vw) of the non-reactive coating was  $8.5 \times 10^{-6} \text{ mm}^3\text{N}^{-1}\text{m}^{-1}$ . The minimum Vw =  $5.0 \times 10^{-6} \text{ mm}^3\text{N}^{-1}\text{m}^{-1}$  was characteristic of the coating obtained at a 12.5 sccm N<sub>2</sub> flow rate. Increasing the nitrogen flow rate to 25 and 37.5 sccm led to increases in Vw by 1.9 and 2.3 times, respectively. It should be noted that the coating obtained at 37.5 sccm N<sub>2</sub> was worn out to the full depth.

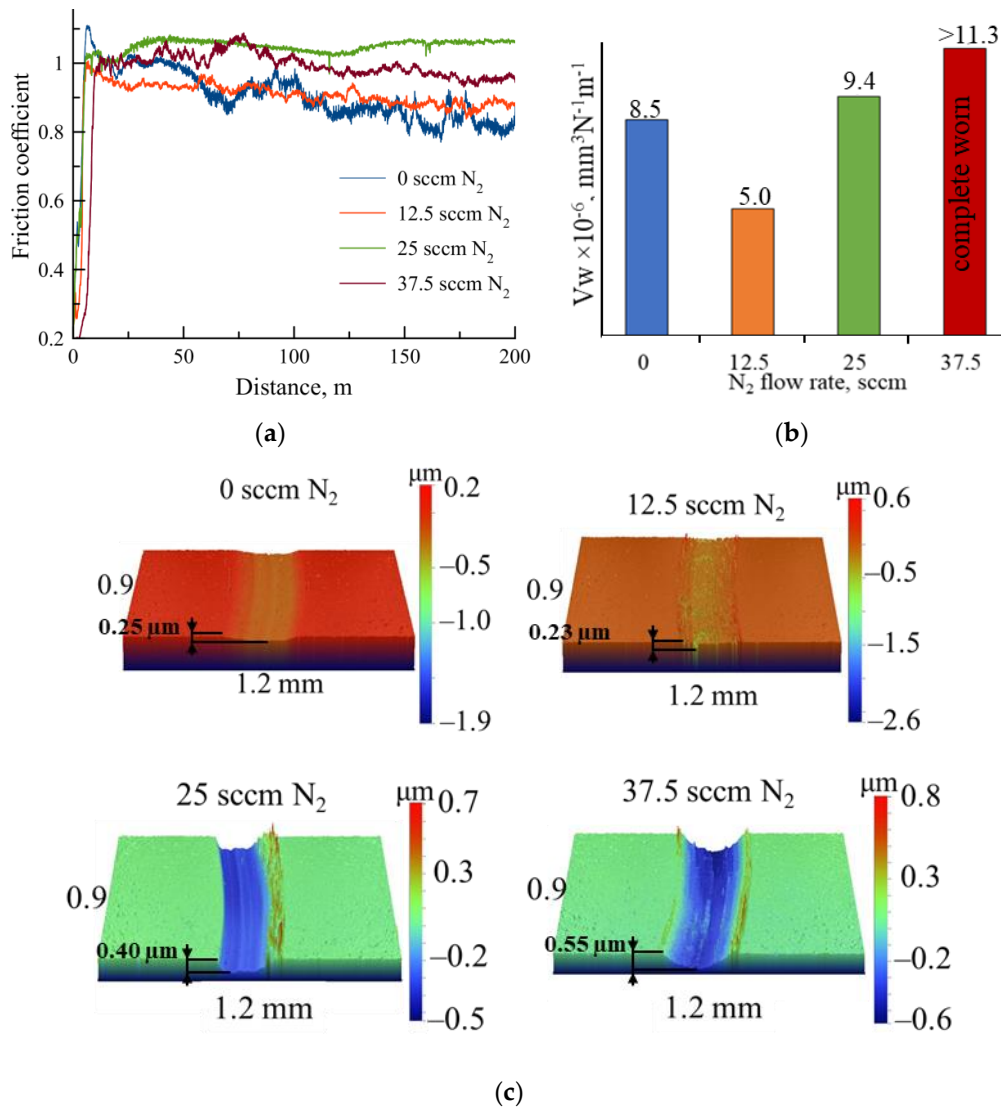


**Figure 6.** The dependence of the friction coefficient on the distance (a), the wear rates vs. nitrogen flow rates (b), and 3D images of the tribocontact zones (c) of Mo-Hf-Y-Si-B-N coatings.

It should be noted that for similar hardness values, the coating obtained at 12.5 sccm had the highest wear resistance compared with the coating deposited at 25.0 sccm. A decrease in wear resistance with an increase in nitrogen consumption can be associated with a high level of residual stress and low adhesive strength. Due to low adhesive strength, the peeled particles of the coating enter the tribocontact zone and have

an additional abrasive effect, as a result of which the wear rate of the coating [48]. A similar decrease in wear resistance with the increase in nitrogen concentration associated with the abrasive effect of wear products is typical of nitride coatings [49].

The curves of the dependence of the specific weight change ( $\Delta m/S$ ) on the oxidation time at a temperature of 1000 °C are shown in Figure 7.

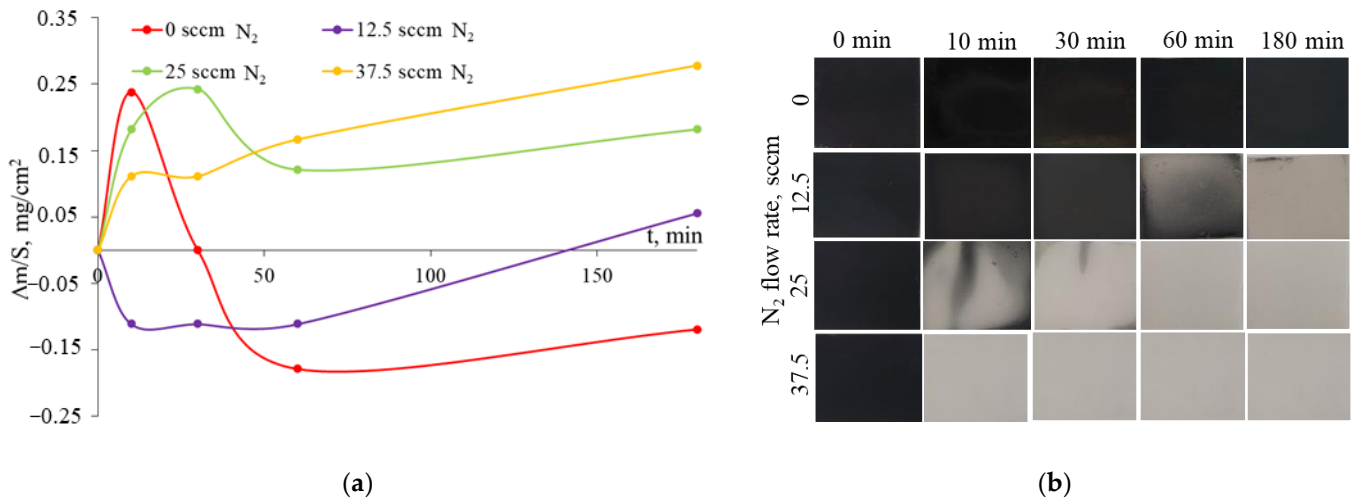


**Figure 7.** Dependence of the specific weight change of the Mo-Hf-Y-Si-B-N coatings on the exposure time (a) at a temperature of 1000 °C and the appearance of the coatings in the as-deposited state and after annealing at 1000 °C (b).

For the non-reactive coating,  $\Delta m/S = 0.24 \text{ mg}/\text{cm}^2$  was observed in the initial time period of 0–10 min, which was associated with the formation of an oxide layer on the coating surface. A further decrease in  $\Delta m/S$  to  $-0.12 \text{ mg}/\text{cm}^2$  after exposure times of 10–180 min can be explained by the formation of volatile oxide  $\text{MoO}_3$  [3,16]. The specific weight of the coating obtained at 12.5 sccm  $\text{N}_2$  was  $-0.11 \text{ mg}/\text{cm}^2$  after exposure times of 10–60 min. After 180 min,  $\Delta m/S$  increased to  $0.06 \text{ mg}/\text{cm}^2$  due to the rapid oxidation of the coating. For coatings deposited at 25.0 and 37.5 sccm  $\text{N}_2$ , an increase in  $\Delta m/S$  was observed at all holding times, which was associated with the formation of an oxide layer on the coating surface.

When analyzing the appearance of the coatings, it was found that the non-reactive coating did not oxidize and retained its integrity during annealing for 10–180 min. In the coating obtained at a nitrogen flow rate of 12.5 sccm, delaminations and oxidation sites were not observed during 10–30 min exposure. With an increase in the exposure time ( $t$ ) to 60 min, the coating was partially oxidized. At  $t = 180 \text{ min}$ , the complete oxidation of the coating was observed with the formation of a transparent oxide layer. The coating deposited at 25.0 sccm  $\text{N}_2$  was partially oxidized at  $t = 10$  and 30 min. Increasing the exposure time to 60 min led to the complete oxidation of the coating. The coating deposited at 37.5 sccm  $\text{N}_2$  was already completely oxidized at  $t = 10 \text{ min}$ . The low resistance to oxidation of nitrogen-containing Mo-Hf-Y-Si-B-N coatings can be associated with the formation of boron and nitrogen oxides when heated in air. These oxides have a high saturation vapor pressure at 800 °C and thus quickly evaporate and destroy the structural integrity of the coatings [50]. Similar results were previously observed in [51,52] during the oxidation of nitride coatings.

Thus, the Mo-Hf-Y-Si-B coating obtained in Ar was characterized by the best oxidation resistance at a temperature of 1000 °C. It should be noted that no delaminations were observed during annealing in all coatings, which indicates their relative high adhesive strength to alumina substrates.

Nitrogen-free coatings are characterized by high oxidation resistance and may be promising for protecting furnace equipment parts. Coatings with optimal composition obtained at 12.5 and 25.0 sccm  $\text{N}_2$ , with high erosion resistance and satisfactory oxidation

resistance, are more suitable for protecting objects subject to wear and heat, such as gas turbine blades. Coatings with the maximum concentration of nitrogen have the potential to be used as antireflection optical coatings.

In further research, it is necessary to minimize the influence of the thickness of Mo-Hf-Y-Si-B-(N) coatings on their operational characteristics. A logical continuation of the work will be the production of Mo-Hf-Y-Si-B-(N) coatings with greater thickness and increased adhesive strength to improve oxidation resistance and determine the critical operating temperature of the coatings. It is also promising to use the HIPIMS method.

#### 4. Conclusions

Mo-Hf-Y-Si-B-N coatings were obtained using direct current magnetron sputtering at nitrogen flow rates varying from 0 to 37.5 sccm.

All coatings had a homogeneous, defect-free structure. The coating growth rate decreased from 270 to 50 nm/min as the N<sub>2</sub> flow rate increased from 0 to 37.5 sccm. The Mo-Hf-Y-Si-B-N coatings were X-ray amorphous. The presence of Mo-Si and Mo-B bonds was revealed in non-reactive coatings. The introduction of nitrogen contributed to the formation of an additional Si-N bond.

The N-free Mo-Hf-Y-Si-B coating was characterized by hardness of 14 GPa. The maximal hardness value of 16 GPa was observed in coatings obtained at nitrogen flow rates of 12.5 and 25.0 sccm. In this case, the elastic modulus decreased from 220 to 130 GPa with an increase in the N<sub>2</sub> flow rate from 0 to 37.5 sccm. The maximum values of  $W = 57\%$ ,  $H/E = 0.098$ , and  $H^3/E^2 = 0.157$  GPa were achieved at a N<sub>2</sub> flow rate of 25 sccm.

Increasing the nitrogen flow rate from 0 to 12.5 sccm led to a decrease in the wear rate from 8.5 to  $5.0 \times 10^{-6}$  mm<sup>3</sup>N<sup>-1</sup>m<sup>-1</sup> under sliding friction conditions.

The best oxidation resistance at 1000 °C was observed in the Mo-Hf-Y-Si-B non-reactive coating.

Thus, Mo-Hf-Y-Si-B-N coatings, which have high mechanical characteristics and wear resistance under conditions of sliding friction, are promising candidates for protecting critical parts of friction pairs, including those operating at elevated temperatures.

**Supplementary Materials:** The following supporting information can be downloaded at: <https://www.mdpi.com/article/10.3390/jcs7060253/s1>, Figure S1: Dependence of the transmittance of Mo-Hf-Y-Si-B-N coatings on the nitrogen flow rate, Figure S2: Micrographs of indentations after mechanical testing of Mo-Hf-Y-Si-B-N coatings at loads of 10 N and 50 N.

**Author Contributions:** Supervision, P.K.-K.; Conceptualization, A.S. and P.K.-K.; formal analysis, A.S. and P.K.-K.; investigation, A.S., F.C., B.S. and P.K.-K.; resources, E.L.; writing—original draft preparation, A.S.; writing—review and editing, P.K.-K. All authors have read and agreed to the published version of the manuscript.

**Funding:** This work was performed with financial support by Russian Science Foundation (project No. 19-19-00117-II). XPS investigations were performed using equipment of Joint Research Center «Material Science and Metallurgy» NUST MISIS, supported by the Ministry of Education and Science of the Russian Federation (project No. 075-15-2021-696).

**Data Availability Statement:** Not applicable.

**Acknowledgments:** The authors are grateful to I. Volkov (Research Laboratory “Inorganic nanomaterials”) for conducting research using Raman spectroscopy.

**Conflicts of Interest:** The authors declare no conflict of interest.

#### References

1. Bahr, A.; Richter, S.; Hahn, R.; Wojcik, T.; Podsednik, M.; Limbeck, A.; Ramm, J.; Hunold, O.; Kolozsvári, S.; Riedl, H. Oxidation Behaviour and Mechanical Properties of Sputter-Deposited TMSi<sub>2</sub> Coatings (TM = Mo, Ta, Nb). *J. Alloy. Compd.* **2023**, *931*, 167532. [[CrossRef](#)]
2. Taylor, M.; Perepezko, J.H. Hot Corrosion of Mo-Si-B Coatings. *Oxid. Met.* **2017**, *87*, 705–715. [[CrossRef](#)]

3. Perepezko, J.H. High Temperature Environmental Resistant Mo-Si-B Based Coatings. *Int. J. Refract. Met. Hard Mater.* **2018**, *71*, 246–254. [[CrossRef](#)]
4. Lemberg, J.A.; Ritchie, R.O. Mo-Si-B Alloys for Ultrahigh-Temperature Structural Applications. *Adv. Mater.* **2012**, *24*, 3445–3480. [[CrossRef](#)] [[PubMed](#)]
5. Terent'eva, V.S.; Zhestkov, B.E. Multifunctional High-Temperature D5 MAI and M1 MAI Coatings. *Russ. J. Phys. Chem. B* **2009**, *3*, 391–396. [[CrossRef](#)]
6. Musil, J.; Zeman, P. Hard A-Si<sub>3</sub>N<sub>4</sub>/MeN<sub>x</sub> Nanocomposite Coatings with High Thermal Stability and High Oxidation Resistance. *Solid State Phenom.* **2007**, *127*, 31–36.
7. Vlček, J.; Potocký, Š.; Čížek, J.; Houška, J.; Kormunda, M.; Zeman, P.; Peřina, V.; Zemek, J.; Setsuhara, Y.; Konuma, S. Reactive Magnetron Sputtering of Hard Si–B–C–N Films with a High-Temperature Oxidation Resistance. *J. Vac. Sci. Technol. A Vac. Surf. Film.* **2005**, *23*, 1513. [[CrossRef](#)]
8. He, J.; Zhang, M.; Jiang, J.; Vlček, J.; Zeman, P.; Steidl, P.; Meletis, E.I. Microstructure Characterization of High-Temperature, Oxidation-Resistant Si–B–C–N Films. *Thin Solid Film.* **2013**, *542*, 167–173. [[CrossRef](#)]
9. Šimová, V.; Vlček, J.; Zuzjaková, Š.; Houška, J.; Shen, Y.; Jiang, J.; Meletis, E.I.; Peřina, V. Magnetron Sputtered Hf–B–Si–C–N Films with Controlled Electrical Conductivity and Optical Transparency, and with Ultrahigh Oxidation Resistance. *Thin Solid Film.* **2018**, *653*, 333–340. [[CrossRef](#)]
10. Farhadizadeh, A.; Vlček, J.; Houška, J.; Haviar, S.; Čerstvý, R.; Červená, M.; Zeman, P.; Matas, M. Effect of Nitrogen Content on High-Temperature Stability of Hard and Optically Transparent Amorphous Hf–Y–Si–B–C–N Coatings. *Ceram. Int.* **2023**, *49*, 6086–6093. [[CrossRef](#)]
11. Kotrlová, M.; Zeman, P.; Houška, J.; Šimová, V.; Procházka, M.; Čerstvý, R.; Haviar, S.; Vlček, J. Enhancement of High-Temperature Oxidation Resistance and Thermal Stability of Hard and Optically Transparent Hf–B–Si–C–N Films by Y or Ho Addition. *J. Non. Cryst. Solids* **2021**, *553*, 120470. [[CrossRef](#)]
12. Kiryukhantsev-Korneev, F.V.; Lemesheva, M.V.; Shvyndina, N.V.; Levashov, E.A.; Potanin, A.Y. Structure, Mechanical Properties, and Oxidation Resistance of ZrB<sub>2</sub>, ZrSiB, and ZrSiB/SiBC Coatings. *Prot. Met. Phys. Chem. Surf.* **2018**, *54*, 1147–1156. [[CrossRef](#)]
13. Kiryukhantsev-Korneev, P.V.; Potanin, A.Y. Structure, Mechanical Properties, and Oxidation Resistance of MoSi<sub>2</sub>, MoSiB, and MoSiB/SiBC Coatings. *Russ. J. Non-Ferrous Met.* **2018**, *59*, 698–708. [[CrossRef](#)]
14. Glechner, T.; Oemer, H.G.; Wojcik, T.; Weiss, M.; Limbeck, A.; Ramm, J.; Polcik, P.; Riedl, H. Influence of Si on the Oxidation Behavior of TM-Si-B<sub>2</sub>±z Coatings (TM = Ti, Cr, Hf, Ta, W). *Surf. Coat. Technol.* **2022**, *434*, 128178. [[CrossRef](#)]
15. Kiryukhantsev-Korneev, P.V.; Iatsyuk, I.V.; Shvindina, N.V.; Levashov, E.A.; Shtansky, D.V. Comparative Investigation of Structure, Mechanical Properties, and Oxidation Resistance of Mo-Si-B and Mo-Al-Si-B Coatings. *Corros. Sci.* **2017**, *123*, 319–327. [[CrossRef](#)]
16. Kiryukhantsev-Korneev, P.V.; Sytchenko, A.D.; Sviridova, T.A.; Sidorenko, D.A.; Andreev, N.V.; Klechkovskaya, V.V.; Polčák, J.; Levashov, E.A. Effects of Doping with Zr and Hf on the Structure and Properties of Mo-Si-B Coatings Obtained by Magnetron Sputtering of Composite Targets. *Surf. Coat. Technol.* **2022**, *442*, 128141. [[CrossRef](#)]
17. Kiryukhantsev-Korneev, P.V.; Kudryashov, A.E.; Sheveyko, A.N.; Orekhov, A.S.; Levashov, E.A. Improving the Oxidation Resistance of Inconel 718 High-Temperature Nickel Alloy Using Combined Surface Engineering Technology. *Lett. Mater.* **2020**, *10*, 371–376. [[CrossRef](#)]
18. Kiryukhantsev-Korneev, P.V.; Pierson, J.F.; Bychkova, M.Y.; Manakova, O.S.; Levashov, E.A.; Shtansky, D.V. Comparative Study of Sliding, Scratching, and Impact-Loading Behavior of Hard CrB<sub>2</sub> and Cr–B–N Films. *Tribol. Lett.* **2016**, *63*, 44. [[CrossRef](#)]
19. Huang, B.; Liu, L.T.; Du, H.M.; Chen, Q.; dan Liang, D.; Zhang, E.G.; Zhou, Q. Effect of Nitrogen Flow Rate on the Microstructure, Mechanical and Tribological Properties of CrAlTiN Coatings Prepared by Arc Ion Plating. *Vacuum* **2022**, *204*, 111336. [[CrossRef](#)]
20. Liu, Z.; Li, H.; Li, J.; Huang, J.; Kong, J.; Wu, Q.; Xiong, D. Microstructure, Mechanical and Tribological Properties of Hf–Mo–Si–N Films with Different Si Contents. *Surf. Coat. Technol.* **2020**, *401*, 126268. [[CrossRef](#)]
21. Auchter, E.; Taylor, M.; Perepezko, J.H. Resistance of a Mo–Si–B-Based Coating to Environmental Salt-Based Hot Corrosion. *Oxid. Met.* **2020**, *93*, 387–399. [[CrossRef](#)]
22. Hou, Q.; Li, M.; Shao, W.; Zhou, C. Oxidation and Interdiffusion Behavior of Mo-Si-B Coating on Nb-Si Based Alloy Prepared by Spark Plasma Sintering. *Corros. Sci.* **2020**, *169*, 108638. [[CrossRef](#)]
23. Deng, X.; Zhang, G.; Wang, T.; Ren, S.; Shi, Y.; Bai, Z.; Cao, Q. Microstructure and Oxidation Resistance of a Multiphase Mo-Si-B Ceramic Coating on Mo Substrates Deposited by a Plasma Transferred Arc Process. *Ceram. Int.* **2019**, *45*, 415–423. [[CrossRef](#)]
24. Zamulaeva, E.I.; Zinovieva, M.V.; Kiryukhantsev-Korneev, P.V.; Petrzhik, M.I.; Kaplanskii, Y.Y.; Klechkovskaya, V.V.; Sviridova, T.A.; Shvyndina, N.V.; Levashov, E.A. Protective Coatings Deposited onto LPBF-Manufactured Nickel Superalloy by Pulsed Electrospark Deposition Using MoSi<sub>2</sub>-MoB-HfB<sub>2</sub> and MoSi<sub>2</sub>-MoB-ZrB<sub>2</sub> Electrodes. *Surf. Coat. Technol.* **2021**, *427*, 127806. [[CrossRef](#)]
25. Chu, C.W.; Jang, J.S.C.; Chen, H.W.; Chuang, T.L. Enhanced Wear Resistance of the Cr-Based Thin Film Coating on Micro Drill by Doping with W–C–N. *Thin Solid Film.* **2009**, *517*, 5197–5201. [[CrossRef](#)]
26. Kiryukhantsev-Korneev, F.V. Possibilities of Glow Discharge Optical Emission Spectroscopy in the Investigation of Coatings. *Russ. J. Non-Ferr. Met.* **2014**, *55*, 494–504. [[CrossRef](#)]
27. Chen, P.Y.; Wang, W.C.; Wu, Y.T. Experimental Investigation of Thin Film Stress by Stoney's Formula. *Measurement* **2019**, *143*, 39–50. [[CrossRef](#)]

28. Zeman, H.; Musil, J.; Zeman, P. Physical and Mechanical Properties of Sputtered Ta–Si–N Films with a High ( $\geq 40$  at %) Content of Si. *J. Vac. Sci. Technol. A Vac. Surf. Film.* **2004**, *22*, 646. [[CrossRef](#)]
29. Musil, J.; Baroch, P.; Vlček, J.; Nam, K.H.; Han, J.G. Reactive Magnetron Sputtering of Thin Films: Present Status and Trends. *Thin Solid Film.* **2005**, *475*, 208–218. [[CrossRef](#)]
30. Heo, S.J.; Kim, K.H.; Kang, M.C.; Suh, J.H.; Park, C.G. Syntheses and Mechanical Properties of Mo–Si–N Coatings by a Hybrid Coating System. *Surf. Coat. Technol.* **2006**, *201*, 4180–4184. [[CrossRef](#)]
31. Ohishi, Y.; Kurosaki, K.; Suzuki, T.; Muta, H.; Yamanaka, S.; Uchida, N.; Tada, T.; Kanayama, T. Synthesis of Silicon and Molybdenum–Silicide Nanocrystal Composite Films Having Low Thermal Conductivity. *Thin Solid Film.* **2013**, *534*, 238–241. [[CrossRef](#)]
32. Wu, R.; Xu, H.; Zhao, Y.; Zha, C.; Deng, J.; Zhang, C.; Lu, G.; Qin, T.; Wang, W.; Yin, Y.; et al. Borophene-like Boron Subunits-Inserted Molybdenum Framework of MoB<sub>2</sub> Enables Stable and Quick-Acting Li<sub>2</sub>S<sub>6</sub>-Based Lithium-Sulfur Batteries. *Energy Storage Mater.* **2020**, *32*, 216–224. [[CrossRef](#)]
33. Degenhardt, U.; Stegner, F.; Liebscher, C.; Glatzel, U.; Berroth, K.; Krenkel, W.; Motz, G. Sintered Silicon Nitride/Nano-Silicon Carbide Materials Based on Pre-ceramic Polymers and Ceramic Powder. *J. Eur. Ceram. Soc.* **2012**, *32*, 1893–1899. [[CrossRef](#)]
34. Prakash, A.; Sundaram, K.B. Optical and XPS Studies of BCN Thin Films by Co-Sputtering of B<sub>4</sub>C and BN Targets. *Appl. Surf. Sci.* **2017**, *396*, 484–491. [[CrossRef](#)]
35. Yang, J.; De Guzman, R.C.; Salley, S.O.; Ng, K.Y.S.; Chen, B.H.; Cheng, M.M.C. Plasma Enhanced Chemical Vapor Deposition Silicon Nitride for a High-Performance Lithium Ion Battery Anode. *J. Power Sources* **2014**, *269*, 520–525. [[CrossRef](#)]
36. Nayak, M.; Lodha, G.S. Optical Response Near the Soft X-Ray Absorption Edges and Structural Studies of Low Optical Contrast System Using Soft X-Ray Resonant Reflectivity. *J. At. Mol. Opt. Phys.* **2011**, *2011*, 1–23. [[CrossRef](#)]
37. Filatova, E.O.; Sakhonenkov, S.S.; Gaisin, A.U.; Konashuk, A.S.; Chumakov, R.G.; Pleshkov, R.S.; Chkhalo, N.I. Inhibition of Chemical Interaction of Molybdenum and Silicon in a Mo/Si Multilayer Structure by the Formation of Intermediate Compounds. *Phys. Chem. Chem. Phys.* **2021**, *23*, 1363–1370. [[CrossRef](#)]
38. Sakhonenkov, S.S.; Filatova, E.O.; Gaisin, A.U.; Kasatnikov, S.A.; Konashuk, A.S.; Pleshkov, R.S.; Chkhalo, N.I. Angle Resolved Photoelectron Spectroscopy as Applied to X-Ray Mirrors: An in Depth Study of Mo/Si Multilayer Systems. *Phys. Chem. Chem. Phys.* **2019**, *21*, 25002–25010. [[CrossRef](#)]
39. Vanegas, P.H.S.; Calderon, V.S.; Alfonso, O.J.E.; Olaya, F.J.J.; Ferreira, P.J.; Carvalho, S. Influence of Silicon on the Microstructure and the Chemical Properties of Nanostructured ZrN–Si Coatings Deposited by Means of Pulsed-DC Reactive Magnetron Sputtering. *Appl. Surf. Sci.* **2019**, *481*, 1249–1259. [[CrossRef](#)]
40. Zhuo, Z.; Sannomiya, Y.; Kanetani, Y.; Yamada, T.; Ohmi, H.; Kakiuchi, H.; Yasutake, K. Interface Properties of SiO<sub>x</sub>N<sub>y</sub> Layer on Si Prepared by Atmospheric-Pressure Plasma Oxidation–Nitridation. *Nanoscale Res. Lett.* **2013**, *8*, 1–6. [[CrossRef](#)]
41. XPS, AES, UPS and ESCA, LaSurface.Com. Available online: <http://www.lasurface.com/database/elementxps.php> (accessed on 15 September 2022).
42. Yuan, Z.; Sun, L.; Fang, Q.; Gong, W.; Wu, X.; Xu, Z. Effect of Nitrogen Flow Rate on Structure and Mechanical Properties of Mo–Al–Si–N Films Prepared by Direct Current Magnetron Sputtering. *Thin Solid Film.* **2015**, *594*, 18–23. [[CrossRef](#)]
43. Musil, J.; Zeman, P.; Baroch, P. Hard Nanocomposite Coatings. *Compr. Mater. Process.* **2014**, *4*, 325–353. [[CrossRef](#)]
44. Khan, A.; Philip, J.; Hess, P. Young’s Modulus of Silicon Nitride Used in Scanning Force Microscope Cantilevers. *J. Appl. Phys.* **2004**, *95*, 1667. [[CrossRef](#)]
45. Wolfenden, A.; Kury, P.B.; Petrovic, J.J. Measurement of Dynamic Young’s Modulus for Molybdenum Disilicide/Pentatitanium Trisilicide. *J. Mater. Eng. Perform.* **1996**, *5*, 232–234. [[CrossRef](#)]
46. Musil, J.; Jirout, M. Toughness of Hard Nanostructured Ceramic Thin Films. *Surf. Coat. Technol.* **2007**, *201*, 5148–5152. [[CrossRef](#)]
47. Ali, R.; Renzelli, M.; Imran Khan, M.; Sebastiani, M.; Bemporad, E. Effects of Residual Stress Distribution on Interfacial Adhesion of Magnetron Sputtered AlN and AlN/Al Nanostructured Coatings on a (100) Silicon Substrate. *Nanomaterials* **2018**, *8*, 896. [[CrossRef](#)] [[PubMed](#)]
48. Holmberg, K.; Ronkainen, H.; Matthews, A. Tribology of Thin Coatings. *Ceram. Int.* **2000**, *26*, 787–795. [[CrossRef](#)]
49. Zhang, K.; Wen, M.; Wang, S.; Deng, R.P.; Gall, D.; Zheng, W.T. Sputter Deposited NbC<sub>x</sub>N<sub>y</sub> Films: Effect of Nitrogen Content on Structure and Mechanical and Tribological Properties. *Surf. Coat. Technol.* **2014**, *258*, 746–753. [[CrossRef](#)]
50. Carminati, P.; Jacques, S.; Rebillat, F. Oxidation/Corrosion of BN-Based Coatings as Prospective Interphases for SiC/SiC Composites. *J. Eur. Ceram. Soc.* **2021**, *41*, 3120–3131. [[CrossRef](#)]
51. Chen, X.; Ma, S.; Xu, K.; Chu, P.K. Oxidation Behavior of Ti–B–C–N Coatings Deposited by Reactive Magnetron Sputtering. *Vacuum* **2012**, *86*, 1505–1512. [[CrossRef](#)]
52. Yang, Y.; Xiao, Q.; Yang, L.; Ren, P.; Li, W.; Zhu, S.; Wang, F. Effect of Nitrogen on High Temperature Oxidation Behavior of AlN-Doped Gradient Coating. *Corros. Sci.* **2022**, *199*, 110155. [[CrossRef](#)]

**Disclaimer/Publisher’s Note:** The statements, opinions and data contained in all publications are solely those of the individual author(s) and contributor(s) and not of MDPI and/or the editor(s). MDPI and/or the editor(s) disclaim responsibility for any injury to people or property resulting from any ideas, methods, instructions or products referred to in the content.